Supplementary Material For

'Comparative stereodynamics in molecule-atom and molecule-molecule rotational energy transfer: NO($A^2\Sigma^+$) + He and D_2.'

Thomas F. M. Luxford,[1] Thomas R. Sharples,[1] Dave Townsend,[1,2] Kenneth G. McKendrick[1] and Matthew. L. Costen[1,a]

[1]*Institute of Chemical Sciences, Heriot-Watt University, Edinburgh, EH14 4AS, U. K.*

[2]*Institute of Photonics & Quantum Sciences, Heriot-Watt University, Edinburgh, EH14 4AS, U. K.*

I. Determination of Collider Speed Distributions

An accurate treatment of the velocity distributions of the two colliders is critical to the extraction of DCS and rotational angular momentum moments from the experimental images. The mean speeds of the NO(A)/Ar and NO(A)/Ne gas mixes used in the He and D_2 experiments, respectively, were determined from fits of 2D Gaussian distributions to images of NO in the molecular beams. These measurements made use of the calibration of arrival position at the detector to velocity, determined as described in the following section. The spread in speeds for a particular set of expansion conditions cannot be reliably extracted from such beam spot images owing to contributions of ion recoil, ion spot size and minor aberrations arising from the ion-optics to the widths of these images. The speed distributions were therefore measured separately in time-of-flight experiments described previously.[1] The NO/Ar beam was found to have a mean speed of 605 ms^{-1} and FWHM 52 ms^{-1} while the NO/Ne beam had mean speed 807 ms^{-1} with FWHM 57 ms^{-1}.

We attempted to determine the speed distributions for the pure He and D_2 beams by various different methods. Speed distributions measured using Gaussian fitting of 'beam-spot' images arising from trace amounts (< 0.01%) of NO seeded in the beams of these colliders yielded simulated images that systematically disagreed with the center position and diameter of the measured scattering images. This suggests that this measurement understates the mean speed of the collider beam, presumably as a result of velocity slip of the heavy NO in the light carrier beam. We also attempted to directly measure the D_2 beam speed distribution using (3+1) REMPI via the D_2 ($B'^1\Sigma_u^+$) state at 267 nm.[2] However, the high ionization recoil velocity imparted to the D_2 (≈ 140 ms^{-1}), resulted in a large uncertainty in the mean D_2 speed obtained from this measurement, and prevented any meaningful attempt to determine the speed distribution. We have therefore determined the mean and FWHM of the (assumed) Gaussian speed distributions for the D_2 and He beams directly by minimizing the residual

[a] Author to whom correspondence should be addressed. Electronic mail: m.l.costen@hw.ac.uk

for fits to the experimental images. For N' = 3, 5-11 mean speeds were found to be 2032 ms^{-1} for D_2 and 1973 ms^{-1} for He, with FWHM of 99 ms^{-1} and 101ms^{-1}, respectively. A substantially higher mean speed of 2026 ms^{-1} was required to satisfactorily fit the experimental data for N' = 12 for collisions with He. This is consistent with this highest observable product state being preferentially formed from collisions between the fastest moving subset of molecules in the NO/Ne and He molecular beams, which was confirmed by the collision-energy dependence of the integral cross section for N' = 12 from the quantum scattering calculations. No similar collision energy dependence was observed for D_2 scattering, for which the N' = 12 images were satisfactorily fitted using the same mean molecular beam speeds as the lower- N'.

II. D_2 molecular beam rotational state populations

We used (3+1) REMPI via the $B'^1\Sigma_u^+$ state at a wavelength of 267-268 nm to study the initial rotational state distribution of the D_2 molecular beam.[2] Measurements were performed on a molecular beam of neat D_2 with a backing pressure of 5 bar, in order to match the conditions of the scattering experiments. The probe laser beam, which had a diameter of 3 mm and a pulse energy of 0.9 mJ, was focussed into the molecular beam by a lens with a focal length of 30 cm. D_2^+ ions formed in the REMPI process were accelerated onto the MCP/phosphor detector, which was gated to exclude ions of other mass-to-charge ratios. The total ion intensity was recorded using an avalanche photodiode which imaged the phosphor, and the wavelength was step-scanned to obtain the spectrum displayed in Fig. 1. The spectrum shows clear lines that may be assigned to R and P branch transitions, but overall has relatively poor signal-to-noise, resulting from the 4-photon REMPI process used. To more accurately determine the relative signal sizes for the R(j) transitions, the wavelength of the laser was fixed at the peak of each of the R(0), R(1) and R(2) transitions in sequence, and velocity mapped images of the D_2 molecular beam spot were acquired, together with background images in the absence of the D_2 molecular beam. The signal and background images were summed over 5000 laser shots, and after subtraction of the summed background image, the D_2 beam spot region of the summed signal image was integrated. The resulting integrated signal levels for the R(0), R(1) and R(2) transitions are given in Table I. There is no literature analysis of the rotational linestrengths in this (3+1) REMPI process, and we have therefore not attempted to turn these relative intensities into relative populations. The observed intensities of j = 0 and j = 2 are consistent with moderate rotational cooling; taking the intensities as populations implies a rotational temperature of ≈ 60 K. The observed intensities of the j = 0 and j = 1 states are broadly consistent with the expected 2:1 ratio arising from the ortho:para ratio of the D_2.

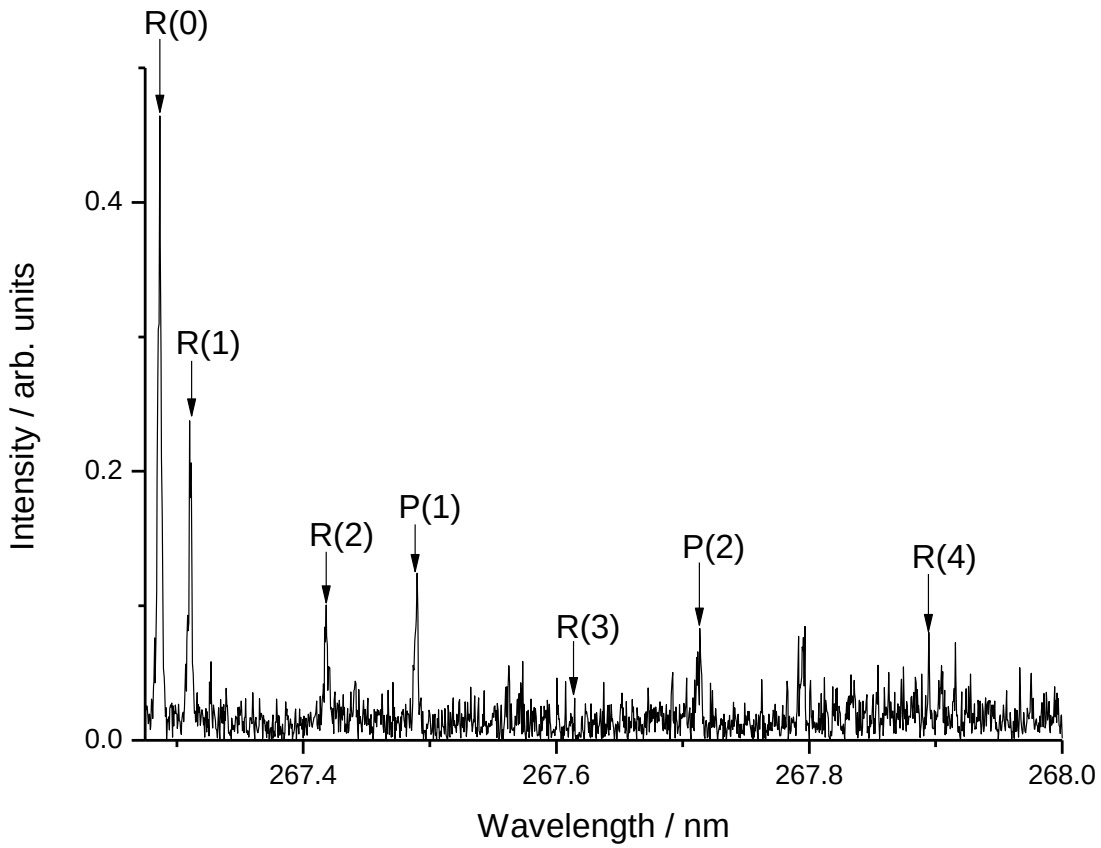

Figure 1: 3+1 REMPI spectrum of the B′-X(0,0) band of D_2, with labels indicating the assigned transitions.

Table 1: Relative intensity of the different transitions in the R-branch of the B′-X(0,0) band of D_2.

Transition	Relative integrated intensity
R(0)	0.682
R(1)	0.257
R(2)	0.061

III. Velocity Calibration of Images

The measurement of velocities directly from images relies on an accurate calibration of arrival position on the detector to laboratory frame velocities, *i.e.* the position on the detector corresponding to zero velocity as well as the difference in velocity corresponding to the separation between two pixels. The method by which this was achieved is described more fully in a previous publication.[1] Briefly, a trace concentration of NO (< 0.01 %) was separately seeded in He, Ne and Ar carrier gases, in order to generate molecular beams with three different mean speeds. (1+1) REMPI of NO at ≈ 226 nm was used to

record images of the velocities of the molecular beams simultaneously produced from both pulsed valves. The resulting images were fitted to 2-D Gaussian distributions to determine the pixel co-ordinates for each molecular beam. These co-ordinates lie along straight lines corresponding to the directions of travel of the molecular beams; the intersection of these lines was identified with the position of zero velocity. This procedure was repeated daily, and the zero position was found to be stable to within 3-4 pixels along each (x, y) image axis over an 8-week period. Experimental scattering images from individual acquisitions on different days were translated prior to analysis and fitting to ensure that the zero-velocity positions of all images coincided. The pixel to velocity ratio was determined from analysis of images of O^+-ions formed from the 226 nm photolysis and photo-ionisation of O_2, as has become conventional in the calibration of VMI experiments.[3-5]

IV. Monte-Carlo Simulation with 3-D Collider Velocities

In our previous analysis, we assumed that the initial collider velocities were constrained to lie exactly along the x and z axes of the laboratory frame. In practice, molecular beams spread out from the skimmer apertures towards the crossing region in a cylindrically symmetric distribution. The pump laser beam intersects the overlapping beams with these two velocity distributions in the centre of the scattering region, bisecting the molecular beams, and selecting a subset of the molecular beam velocities. We model the pump laser beam as a cylinder of uniform intensity, with a radius of 1 mm and length of 6 mm, the latter defined by the overlap with the ionization laser beam, which propagates orthogonal to the pump laser beam. We have modelled the collision velocities on the assumption that collisions occur between NO molecules and collision partners within this pump volume, with initial velocities that originate at the orifice of the pulsed valves and project through the respective skimmers. For each scattering event in the Monte-Carlo simulation, a point was chosen within this pump laser beam volume, and trajectories were propagated back to randomly chosen points within the 0.5 mm orifices of each of the pulsed valves. Each trajectory was then tested to ensure that it passed through its respective skimmer. The resulting successful initial trajectories were then combined with the speeds Monte-Carlo selected from the appropriate Gaussian speed distribution to yield initial NO and collider velocities for that simulated event.

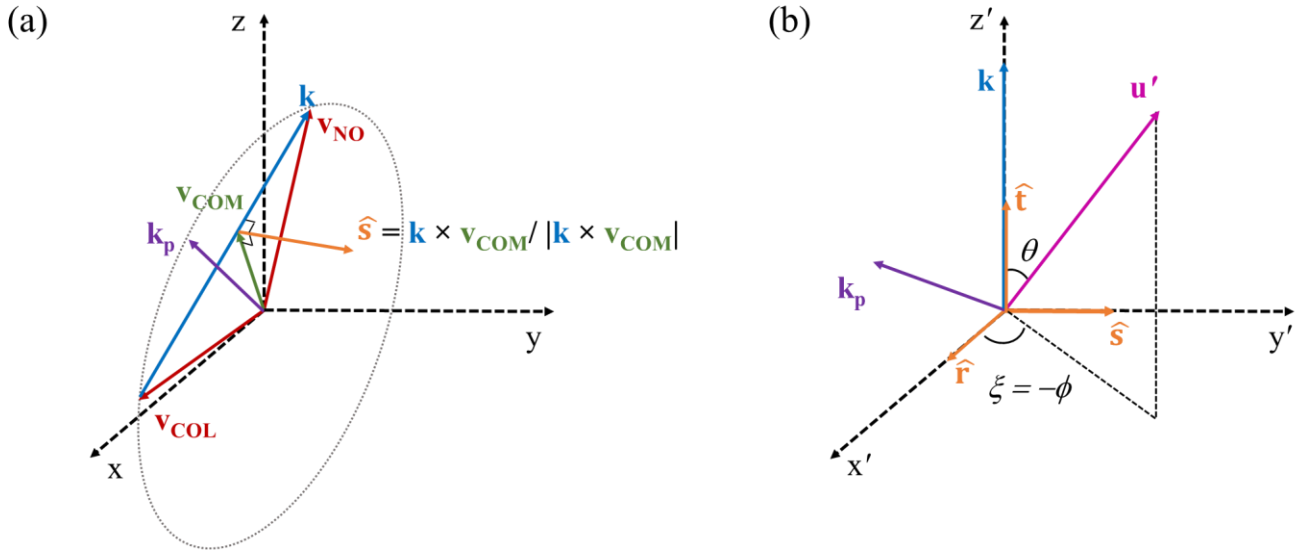

Figure 2: (a) The laboratory frame (x,y,z), defined such that the z and x axes lie parallel to the axes of cylindrical symmetry of the NO and collider velocity distributions, respectively. The coplanar vectors $\mathbf{v}_{NO}$, $\mathbf{v}_{COL}$, $\mathbf{k}$, $\mathbf{v}_{COM}$ and $\mathbf{k}_p$ discussed in the text are indicated as well as the unit vector $\hat{\mathbf{s}}$, which is perpendicular to the plane in which these five vectors lie. (b) The frame (x′,y′,z′) defined such that the z′ lies parallel to $\mathbf{k}$ and the x′z′ frame contains $\mathbf{v}_{NO}$, $\mathbf{v}_{COL}$ and $\mathbf{k}_p$. The unit vectors $\hat{\mathbf{r}}$, $\hat{\mathbf{s}}$ and $\hat{\mathbf{t}}$ lying along the three axes of this frame are indicated as well as the scattered NO center of mass velocity $\mathbf{u}'$.

Selecting the initial velocities in this fashion results in initial relative collision velocities, $\mathbf{k}$, and center of mass velocities, $\mathbf{v}_{COM}$, that are not constrained to lie in the plane of the VMI image, in contrast to our assumptions in earlier work. Figure 2 (a) illustrates the experimental laboratory frame (x,y,z), which is defined by the cylindrical symmetry axes of the collider initial velocity distributions such that z lies along the NO molecular beam axis and x lies along the collider beam axis. The origin for this frame lies at zero velocity in the laboratory frame. The initial laboratory frame velocities of NO, $\mathbf{v}_{NO}$, and the He/D_2 collider, $\mathbf{v}_{COL}$, define a scattering plane in which $\mathbf{k}$ and $\mathbf{v}_{COM}$ also lie.

Figure 2 (b) shows a second frame of reference (x′,y′,z′) defined with origin $\mathbf{v}_{COM}$. The z′ axis lies parallel to $\mathbf{k}$ and the x′z′ plane is defined to contain $\mathbf{v}_{NO}$ and $\mathbf{v}_{COL}$. This plane is therefore parallel to the plane containing $\mathbf{v}_{NO}$, $\mathbf{v}_{COL}$, $\mathbf{k}$ and $\mathbf{v}_{COM}$ illustrated in Figure 2 (a). The polar angle describing the direction of $\mathbf{u}'$ in this frame is the scattering angle θ, and we denote the azimuthal angle ξ. The final center-of-mass-referenced NO velocity may be written as:

$$\mathbf{u}' = \sin\theta\cos\xi\,\hat{\mathbf{r}} + \sin\theta\sin\xi\,\hat{\mathbf{s}} + \cos\theta\,\hat{\mathbf{t}}$$

where $\hat{\mathbf{r}}$, $\hat{\mathbf{s}}$ and $\hat{\mathbf{t}}$ are unit vectors along the x′, y′ and z′ axes, respectively. Since $\hat{\mathbf{t}}$ is parallel to **k**, and $\hat{\mathbf{s}}$ is perpendicular to both **k** and $\mathbf{v}_{COM}$, the unit vectors $\hat{\mathbf{r}}$, $\hat{\mathbf{s}}$ and $\hat{\mathbf{t}}$ may be calculated straightforwardly:

$$\hat{\mathbf{t}} = \mathbf{k} / |\mathbf{k}|$$

$$\hat{\mathbf{s}} = \mathbf{k} \times \mathbf{v}_{COM} / |\mathbf{k} \times \mathbf{v}_{COM}|$$

$$\hat{\mathbf{r}} = \hat{\mathbf{s}} \times \hat{\mathbf{t}}$$

Once the laboratory frame components of these unit vectors are known, the laboratory frame final velocity **v'** is:

$$\mathbf{v'} = \mathbf{u'} + \mathbf{v}_{COM} = \sin\theta\cos\xi\,\hat{\mathbf{r}} + \sin\theta\sin\xi\,\hat{\mathbf{s}} + \cos\theta\,\hat{\mathbf{t}} + \mathbf{v}_{COM}$$

In treating the angular momentum polarization sensitivity of the probe scheme we make the simplifying assumption that the propagation direction of the probe laser $\mathbf{k}_p$ lies in the scattering plane defined by $\mathbf{v}_{NO}$ and $\mathbf{v}_{COL}$ with the polarization of the probe laser lying parallel and perpendicular to this plane for H and V polarization geometries, respectively. This is a very good approximation: the maximum angle between **k** and the laboratory xz plane in the 10^7 trajectories sampled in the Monte-Carlo simulation was 0.43° for the NO(A) + He experiments, and 0.49° for the NO(A) + D_2 experiments, while we estimate the precision to which the alignment of the polarization optics in the laboratory frame may be set to be ±1°. Under this assumption, the x′z′ plane contains $\mathbf{k}_p$, such that the (x′,y′,z′) frame of reference may be obtained from the scattering frame of reference, in which the angular momentum polarization moments are defined, by rotation through the Euler angles (-ϕ,0,0),[6] where ϕ is the azimuthal angle describing the direction of $\mathbf{k}_p$ in the scattering frame, and $\xi = -\phi$. This simplifying approximation is consistent with the approach of Brouard and co-workers, and enables us to retain the polarization sensitivity analysis used in our previous work.[1, 7]

V. NO($A^2\Sigma^+$) – He Potential Energy Surface

The quantum scattering calculations were performed on the *ab initio* potential energy surface (PES) calculated at RCCSD(T) level by Kłos *et al.*[8] Figure 3(a) shows a polar contour plot of this PES, illustrating the 'soft' repulsive wall referred to in the

main text. Only the anisotropic elements of the PES are capable of causing rotational energy transfer, and the PES is used in the quantum scattering calculations as an expansion of radial terms expressing the contribution of different orders, λ, of the Legendre moments, $P_\lambda(\cos\theta)$, where θ is the polar angle between the NO bond axis $\boldsymbol{r}_{NO}$ and the intermolecular He-NO vector, $\boldsymbol{R}$. Figure 3(b) shows these radial functions for the Legendre moments with λ = 0 – 6. Since the original PES single point energies were calculated at only 7 discrete angles (θ = 0°, 30°, 60°, 90°, 120°, 150° and 180°), only 7 Legendre moments are required to describe the PES.

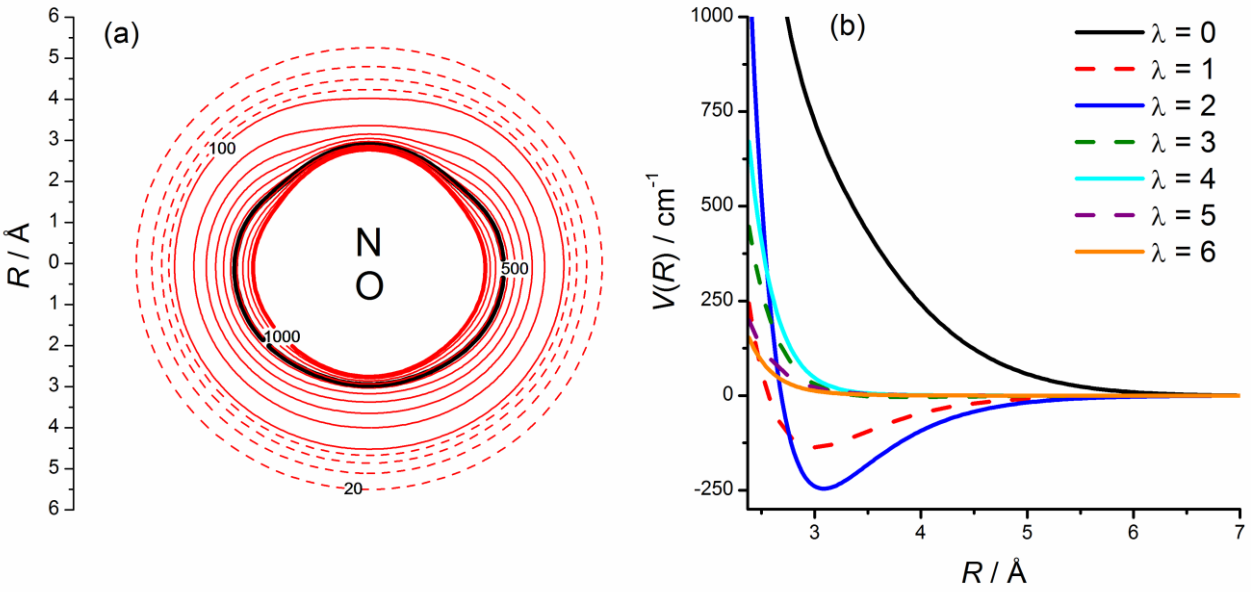

Figure 3: *(a) Polar contour plot of the NO(A)-PES from Ref. 8. Dashed red contours; 20 cm^{-1} intervals from 20 to 80 cm^{-1}. Solid red contours; 100 cm^{-1} intervals from 100 to 1000 cm^{-1}. Solid black contour; 670 cm^{-1}, representing average collision energy in the experiments presented in this paper. (b) Radial dependence of the Legendre moments of the PES.*

References

1. T. R. Sharples, T. F. M. Luxford, D. Townsend, K. G. McKendrick, and M. L. Costen, J Chem Phys **143**, 204301 (2015).
2. S. T. Pratt, P. M. Dehmer, and J. L. Dehmer, J Chem Phys **86**, 1727 (1987).
3. D. H. Parker and A. T. J. B. Eppink, J Chem Phys **107**, 2357 (1997).
4. J. J. Lin, J. G. Zhou, W. C. Shiu, and K. P. Liu, Rev Sci Instrum **74**, 2495 (2003).
5. G. R. Wu, W. Q. Zhang, H. L. Pan, Q. Shuai, B. Jiang, D. X. Dai, and X. M. Yang, Rev Sci Instrum **79**, 094104 (2008).
6. R. N. Zare, *Angular Momentum: Understanding Spatial Aspects in Chemistry and Physics* (Wiley, New York, 1988).
7. M. Brouard, H. Chadwick, C. J. Eyles, B. Hornung, B. Nichols, F. J. Aoiz, P. G. Jambrina, and S. Stolte, J Chem Phys **138**, 104310 (2013).
8. J. Kłos, M. H. Alexander, R. Hernandez-Lamoneda, and T. G. Wright, J Chem Phys **129**, 244303 (2008).